Bulletin of Earthquake Engineering
https://doi.org/10.1007/s10518-023-01634-w

ORIGINAL ARTICLE

Displacement incompatibility shape functions between masonry infill wall panels and reinforced concrete frames

Livio Pedone[1] · **Stefano Pampanin**[1]

Received: 19 September 2022 / Accepted: 25 January 2023

Abstract
During an earthquake, the detachment and local interaction between infill wall panels and surrounding frame can occur, potentially leading to significant local damage to both structural and non-structural elements, if not global collapse. Yet, a procedure to assess the relative deformation mechanism in terms of detachment shape and values, rather than, and in addition to, the diagonal compression strut mechanism and associated internal panel strain and stress path, is still missing in the literature. Therefore, in this paper the concept of shape functions is proposed and adopted to assess the seismic displacement incompatibility between infill walls and the surrounding frame structure. A parametric study on different typologies of infilled frames is developed to investigate the key parameters affecting the infill-frame detachment. The proposed concept of shape functions can support the design/retrofit of improved construction details, such as shear keys and/or steel dowels, in view of either decoupling or strengthening retrofit/repair strategies. Moreover, as infill-frame detachment can lead to damage to energy enhancement rehabilitation solutions, such as external thermal insulation systems, which are becoming more common nowadays in view of the international target towards a significant reduction of energy consumption and CO_2 emission, it is suggested to implement the proposed displacement-compatible design check to assess and detail for adequate displacement capacity.

Keywords Displacement incompatibility · Shape functions · Infill walls · Reinforced concrete buildings · Infilled frame structures

1 Introduction and motivation

Reinforced Concrete (RC) frame structures with masonry infill walls represent a large part of the European building stock. Infill wall panels are usually considered as "non-structural" elements as they are designed to provide facade multi-purpose functions (e.g., thermal and acoustic insulation), thus they are often neglected in the structural design. However, it is

✉ Livio Pedone
livio.pedone@uniroma1.it

[1] Department of Structural and Geotechnical Engineering, Sapienza University, 00184 Rome, Italy

Published online: 08 February 2023

well known that infills and surrounding frames have a strong interaction during seismic shakings. Although infilled frame structures exhibit, in a first stage, a significant increase in the lateral strength and stiffness when compared to the bare frame solution, the infill-to-frame seismic interaction can lead to local shear failures of structural elements (Fig. 1a) or global failure mechanism (e.g., soft-story mechanism, Fig. 1b) (Magenes and Pampanin 2004). Moreover, past studies (Taghavi and Miranda 2003; Cardone and Perrone 2017) pointed out that approximately 80% of building loss is associated with damage to non-structural components (e.g., masonry infills, partitions) and contents.

On the other hand, the recent sustainability requirements in European regions (Directive 2018/844 2018) have led to growing attention to the overall performance of facade elements. In Europe, buildings are responsible for 40% of EU energy consumption and 36% of CO_2 emissions (Calvi et al. 2016); therefore, improving structural/seismic safety and energy efficiency of existing buildings has become an important socio-economic and environmental need (Bournas 2018). To achieve this goal, it is becoming increasingly evident that energy and seismic retrofitting should be studied through an integrated multi-performance design approach (Calvi et al. 2016; Marini et al. 2017; Di Vece and Pampanin 2019). Consequently, the seismic performance of facades plays a crucial role since damage to these components can lead to loss of performance to energy refurbishment solutions even for low-intensity earthquakes (Fig. 1c).

Seismic response of infilled RC structures has been widely studied in the past years and effective retrofit solutions capable to reduce the infill-frame seismic interaction have been proposed (e.g., Tsantilis and Triantafillou 2018; Morandi et al. 2018b; Tasligedik and Pampanin 2017; Marinković and Butenweg 2019, 2022). In the case of seismic load, partial detachment between infill panels and surrounding frame occurs, with a concentration of the compression contact region at the diagonally opposite corners, leading to the formation of a diagonal compression strut load path mechanism (Zamic and Tomazevic 1984). In the past, particular focus has been given to the study of the diagonal compression strut load path, with comprehensive experimental and investigation aiming at characterizing its properties (width, depth, contact regions, strength and hysteresis loop, local mechanisms).

Yet, looking at the same interaction mechanism from an alternative and complementary perspective, infill-frame detachment can be harmful to External Thermal Insulation Composite Systems (ETICS) as insulation materials can exhibit a brittle failure when subjected to tensile stresses (Tang et al. 2019). Moreover, seismic retrofit solutions for facade

a) b) c)

Fig. 1 Observed damage to infilled frame structures: **a** shear failure of column (Bonefro, Molise 2002; Magenes and Pampanin 2004); **b** soft story mechanism (Izmit, 1999, NISEE image collection); **c** damage to masonry infill walls and external thermal insulation due to an earthquake (available online: http://www.reluis.it/images/stories/webinar-23-11-20/Prota-daPorto.pdf)

components based on strengthening or decoupling techniques would require appropriate structural details, such as shear anchors or steel dowels, to create a composite action or to decouple the two systems while preventing the out-of-plane collapse of the infill panels. These structural details may damage the facade components or result themselves damaged due to the infill-frame detachment process or displacement incompatibility. Therefore, a better understanding of the displacement incompatibility and detachment mechanism between frame and infill panel, supported by specific investigations, is needed.

In this context, this paper aims to assess the detachment shape and values due to the seismic displacement incompatibility between frame and infill wall by adopting the concept of shape functions. Firstly, a brief review of the modelling approach for infilled frames is provided, and initial parametric analyses are performed to assess the seismic response of different typologies of masonry infills through alternative macro-modelling approaches. Secondly, displacement incompatibility is investigated by developing shape functions for different infilled frame configurations. A simplified modelling approach to assess the value of detachment along the frame structure is adopted and preliminary shape functions are presented. Finally, a conceptual framework to support the assessment and design of specific construction details for decoupling/strengthening' retrofit strategies and techniques, as well as for mechanical fixing systems for external thermal insulation composite systems, is presented.

2 Modelling approaches for masonry infilled frames: literature review

Modelling methods to assess the seismic performance of infilled RC frames can be grouped into: (1) micro-modelling, (2) macro-modelling approaches and (3) meso-modelling approaches. The micro-modelling approach aims to provide an accurate description of the structural behaviour of the infill wall by modelling masonry units and mortar joints in detail. However, this method requires a great amount of data, resulting to be complex and time-consuming for its high computation effort. Otherwise, in the macro-modelling approach there is no distinction between mortar joints and bricks and an equivalent diagonal strut is typically adopted to model the infill panel. Following the meso-modelling approach, the infill panel is idealized as a continuous bi-dimensional element with no distinction between brick–mortar joints. Therefore, the micro-modelling and meso-modelling approaches are generally recommended to investigate local effects due to the infill-frame interaction, while the macro-modelling approach is recommended to assess the global behaviour of the structure, taking advantage of its low computational effort. A state-of-art of different macro-modelling techniques is presented below, since as a first step the equivalent strut model is adopted to achieve the goals of this paper.

Polyakov (1960) was possibly the first author to suggest that the behaviour of infill panels could be described by diagonal struts connected to the two opposite corners of the surrounding frame, while Holmes (1961) firstly applied this concept. The geometrical properties of the equivalent strut are fully described by the thickness of the infill panel t_w, the width b_w and the length of the diagonal strut d_w. The main issue of adopting such an approach is related to the calculation of the width, since the thickness and the length are automatically defined by the panel geometry. Thus, Holmes (1961) proposed an empirical formula to calculate b_w. After a few years, Stafford Smith (1967) developed a mathematical expression to calculate the relative stiffness between infill and frame (λ). The same author also proposed a formulation, widely adopted nowadays, to evaluate the contact

length between panel and frame based on the analogy of a beam on an elastic foundation. Later, other researchers proposed different equations to calculate the equivalent strut width depending on λ, including Mainstone (1974) (adopted by FEMA 306, 1998), Liauw and Kwan (1984), and Decanini and Fantin (1987). It is also acknowledged the work developed by Paulay and Priestley (1992), who proposed a simplified formulation to calculate b_w, as well as the research by Papia et al. (2003), who defined a mathematical expression depending on an alternative relative panel-to-frame-stiffness parameter λ^*. In the model proposed by Bertoldi et al. (1993), adopted in this paper, the strut proprieties are evaluated considering four different failure mechanisms: (1) compression failure at the centre of the infill, (2) compression failure at the corners of the infill, (3) sliding shear failure, and (4) diagonal tension failure. The ultimate compression stress is defined as the minimum value obtained for the four failure mechanisms. The whole formulations for this model are reported in Table 1.

Furthermore, two main different types of equivalent diagonal strut modelling can be identified from a literature review: single diagonal strut models and multiple diagonal strut models. The multiple strut models mainly differ in number, type, inclination, and connection position along the frame of the struts (e.g., Chrysostomou et al. 2002; El-Dakhakhni et al. 2003; Crisafulli and Carr 2007; Di Trapani et al. 2018).

By comparing different diagonal strut models (single, double, and triple strut) with a more refined FEM model, Crisafulli et al. (2000) demonstrated that the single diagonal strut model generally allows to assess the seismic global performance of the structure, however, it is less accurate in capturing the actual distribution of the internal actions expected from the infill–frame interaction. Alternatively, the double and triple diagonal strut models can provide a better estimation of the frame bending moment diagrams.

Although out of the scope of this research work, when dealing with the seismic performance of infilled frame structures, the out-of-plane (OOP) response of infills is also deemed a critical issue, as well as the interaction between the in-plane (IP) and OOP response. Clearly, during seismic shakings, the structure is simultaneously subjected to both IP and OOP loading, and damage to infills due to the IP seismic loads could lead to

Table 1 Formulations of the equivalent strut model proposed by Bertoldi et al. (1993)

$$E_{w\vartheta} = \left[\frac{\cos^4\vartheta}{E_{wh}} + \frac{\text{sen}^4\vartheta}{E_{wv}} + \cos^2\vartheta sen^2\vartheta\left(\frac{1}{G} - \frac{2\upsilon}{E_{wv}}\right)\right]^{-1}$$

$$\lambda = h\left[\frac{E_{w\vartheta}t_w sin2\vartheta}{4E_c I_c h_w}\right]^{1/4} \qquad \frac{b_w}{d_w} = \frac{K_1}{\lambda h} + K_2$$

$$\begin{cases} K_1 = 1.300,\ K_2 = -0.178 & if\ \lambda h \le 3.14 \\ K_1 = 0.707,\ K_2 = 0.010 & if\ 3.14 < \lambda h < 7.85 \\ K_1 = 0.470,\ K_2 = 0.040 & if\ \lambda h \ge 7.85 \end{cases}$$

$$\sigma_{w1} = \frac{1.12 f_{wv} sen\vartheta cos\vartheta}{K_1(\lambda h)^{-0.12} + K_2(\lambda h)^{0.88}}$$

$$\sigma_{w2} = \frac{1.16 f_{wv} tan\vartheta}{K_1 + K_2\lambda h}$$

$$\sigma_{w3} = \frac{(1.2 sen\vartheta + 0.45 cos\vartheta) f_{wu} + 0.3\sigma_v}{b_w/d_w}$$

$$\sigma_{w4} = \frac{0.6 f_{ws} + 0.3\sigma_v}{b_w/d_w}$$

$E_{w\vartheta}, E_{wh}, E_{wv}$, Elastic modulus of the infill in the diagonal, horizontal and vertical direction, respectively; ϑ, Inclination of the strut: G, Shear modulus of the infill; υ, Poisson modulus of the infill; λ, Relative stiffness between infill and frame (Stafford Smith 1967); E_c, Elastic modulus of concrete; I_c, Column moment of inertia; h_w, Height of the infill panel; t_w, b_w, d_w, Thickness, width and length of the diagonal strut, respectively; f_{wh}, Compression strength for the horizontal direction; f_{wv}, Compression strength for the vertical direction; f_{wu}, Sliding shear resistance of the mortar joints;f_{ws}, Shear resistance under diagonal compression; σ_v, Vertical compression stress due to gravity loads; $\sigma_{w1,2,3,4}$, Compression at the centre of the infill, compression at the corners of the infill, sliding shear failure and diagonal tension failure.

a reduction in terms of OOP capacity and vice versa, potentially leading to the collapse of the infill. This topic has been widely studied in the past through both experimental (e.g., Calvi and Bolognini 2001; Furtado et al. 2016; Ricci et al. 2018; Morandi et al. 2022) and numerical (e.g., Cavaleri et al. 2020) investigations. Among others, the results presented by Ricci et al. (2018) can be considered to better understand the IP-OOP interaction in masonry infill panels. Specifically, three infilled RC frames (2:3 scaled), designed according to modern seismic-code provisions in Italy, were tested by applying OOP loads after IP cyclic tests. The three specimens were subjected to an initial IP interstorey drift ratio equal to 0.16%, 0.37%, and 0.58%, respectively; the results were compared to previous experimental investigations carried out by the same authors on a nominally identical specimen subjected to "pure" (i.e., without IP initial damage) OOP loading (Di Domenico et al. 2019). Concerning the OOP strength capacity, a significant reduction was observed when considering initial IP damage, especially for higher initial interstorey drift values: reductions up to -52% and -73% were observed considering an initial interstorey drift equal to 0.37%, and 0.58%, respectively. Recently, some macro-modelling approaches have been proposed for the simulation of the IP and OOP response of infilled frame structures subjected to earthquakes (e.g., Di Trapani et al. 2018; Mazza 2019; Donà et al. 2022).

Finally, the hysteretic behaviour of the infill panel needs to be defined in order to describe its strength and stiffness degradation. Crisafulli (1997) proposed a refined analytical formulation (adopted in this paper) of the backbone curve and hysteresis rule based on the observation of experimental tests on masonry panels.

3 Methodology

Displacement incompatibility for RC frame structures is a well-known issue in seismic engineering and it has been investigated in past research works. However, these works mainly focused on the seismic displacement incompatibility between structural components (e.g., the "beam elongation", Fenwick and Megget 1993; Peng et al. 2011; vertical displacement incompatibility between beams and precast flooring unit, Matthews et al. 2003; Vides and Pampanin 2015). On the other hand, very few studies have focused on the assessment of the infill-frame interaction in terms of contact and, in turn, the complementary detachment zones. Crisafulli (1997) discussed through numerical investigations the relative deformation mechanism between the infill and surrounding frame; particular attention has been given to the modification of the bending moment and shear diagram in the structural members due to the presence of the infill, both in the case of intact panels and panel with horizontal shear sliding failure. Brodsky et al. (2018) investigated the interaction behaviour in terms of the infill-frame contact regions and interfacial tractions in case of loss of a supporting column. Milanesi et al. (2018a) numerically investigated the local seismic interaction between Autoclaved Aerated Concrete (AAC) masonry infills and surrounding RC frames. The authors performed nonlinear static analyses adopting a 'meso-modelling' approach. A comparison between the bare and the infilled frame in terms of moment and shear demand in the columns was provided, highlighting that substantial differences in the distribution of the internal forces were obtained, even for low levels of interstorey drift. Moreover, considering higher interstorey drift values, a higher contact length between infill and frames was observed. The authors also concluded that analytical expressions available in the literature tend to underestimate the contact length of about 50% with respect to the obtained numerical results. Wararuksajja et al. (2020) studied the

local seismic interaction between RC frames and concrete block infill walls through both experimental and numerical investigations in order to provide a design methodology to avoid local brittle failures in the structural members. The increment of shear force in the columns due to the infill-frame interaction has been experimentally evaluated by measuring the strain of the stirrups through uniaxial strain gauges. Results showed that, for interstorey drift values higher than 0.75%, the strain values in the transversal reinforcements increased significantly, especially for strain gauges located at approximately 3/4 of the effective depth of the column (measured from the joint interface). The authors concluded that the corner crushing in the infills can lead to a "short column" mechanism, especially in the case of strong infills, and, consequently, increasing shear demand can be observed, potentially leading to brittle failure mechanisms in the columns. Pashaie and Mohammadi (2021) presented an extended multiple-strut model for infilled steel frames considering different typologies of beam-to-column connection (i.e., rigid, semi-rigid, and pinned). The authors carried out an extensive parametric investigation on refined finite element models characterized by different aspect ratios, friction coefficients, and relative stiffness between infill and frames. Particular focus was given to the ability of the proposed macro-model in estimating the modification of the bending moment diagram in beams and columns due to the infill panel and the three different considered connections. Recently, Facconi and Minelli (2020) studied a strengthening technique for RC weak infilled frames by using thin glass fiber mesh reinforced mortar overlays. The authors paid particular attention to the steel dowel connection between the masonry panel and the RC frame and investigated the different responses of the infill-to-frame interface at different loading levels.

In this work, in order to assess the infill-frame detachment, the concept of displacement compatibility shape functions, introduced by Taylor (2004) and further developed and applied by Vides and Pampanin (2015) to study the vertical displacement incompatibility profiles between the seismic resisting frame and the precast flooring unit, is adopted. Shape functions are defined as the envelope of the maximum (both horizontal and vertical) displacement incompatibility recorded along the interface with the surrounding structural frame.

In order to evaluate the detachment values between the infill wall and surrounding frame structure, the best approach would arguably be to perform a refined model according to micro-modelling techniques. However, as mentioned above, this method requires the identification of several parameters, consequently leading to an excessive effort. It is worth noting that this paper aims to investigate which parameters strongly affect displacement incompatibility as well as to provide a preliminary range of values of detachment expected for different infilled frame configurations. Hence, to achieve this scope, a more simplified modelling approach is adopted. Specifically, a comparative procedure between two different models for the same structural system is carried out, as described in Cavaleri and Di Trapani (2015) where the same method was adopted to predict additional shear actions on frame members due to infills. For each analyzed configuration, two different models are implemented: an equivalent strut model and a continuous bi-dimensional shell model. These models can be considered as equivalent when they exhibit the same lateral secant stiffness under monotonic loading. Hence, operatively the non-linear behaviour of the shell elements is introduced by iteratively reducing their thickness. This procedure aims to obtain for the continuous model the same lateral secant stiffness of the equivalent strut model for a fixed interstorey drift level, as shown in Fig. 2.

It is highlighted that, by a comparison between the multistage linear equivalent bi-dimensional model and a fully nonlinear bi-dimensional model, Cavaleri and Di Trapani (2015) proved that this modelling strategy can provide good accuracy in assessing both

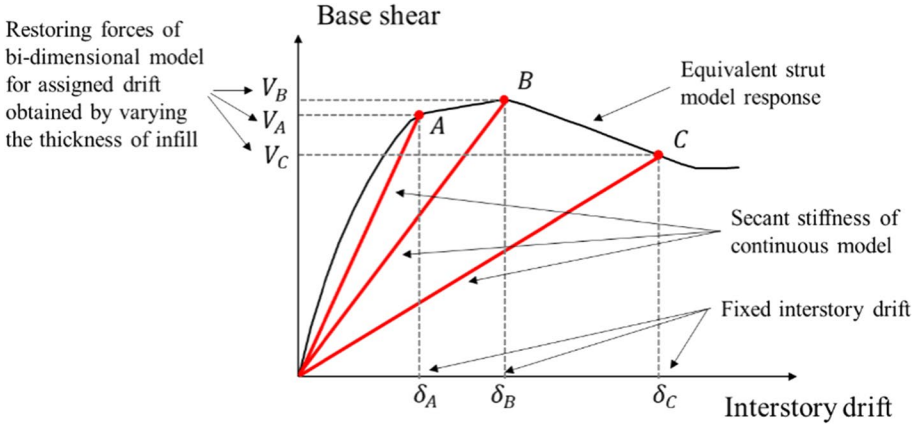

Fig. 2 Theoretical representation of the adopted modelling strategy (after Cavaleri and Di Trapani 2015)

the global response of the structure and the local shear demands on frames. Hence, the structural responses of the two models at specific interstorey drifts are compared. Finally, horizontal and vertical displacements of both structural frame and infill edges are evaluated and shape functions of the displacement incompatibility for a fixed interstorey drift are developed (Fig. 3).

Referring to the adopted modelling strategies, a single strut model seems to be the best choice to assess the global seismic performance of infilled frames. Crisafulli et al. (2000) proved this consideration by performing a comparative analysis of different strut modelling techniques and assuming linear elastic behaviour. However, the more accurate estimation of the frame bending moment diagram derived by double or triple diagonal strut models can modify the nonlinear behaviour of the structure. Therefore, a preliminary parametric

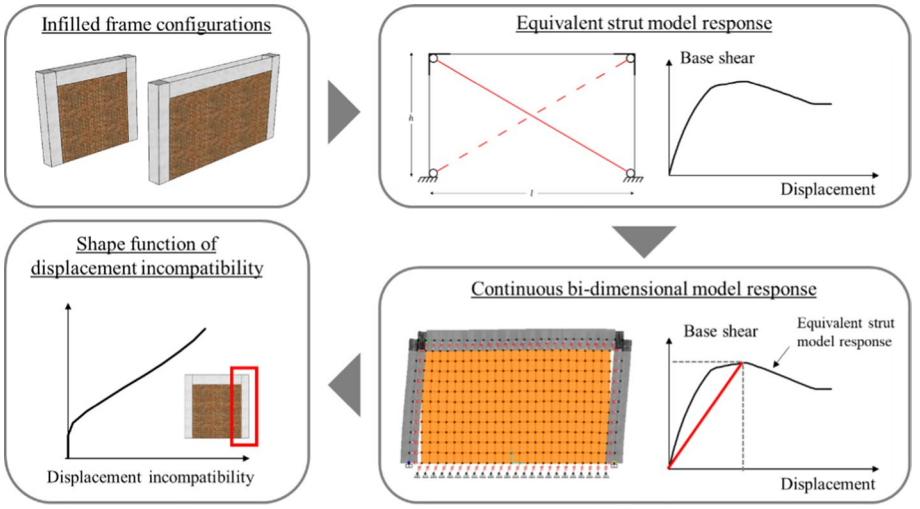

Fig. 3 Flowchart of the adopted methodology to evaluate the displacement-incompatibility shape functions

analysis of the seismic behaviour of infilled frames is also performed to support the choice of the modelling technique.

4 Preliminary parametric analysis of macro-modelling approaches

4.1 Case-study infilled frame structures

Two single-story one-span infilled frame structures, consisting of a bay length of 3 m and 5 m, respectively, and an interstorey height of 3 m, are considered to implement the study. Construction details are typical of a pre-1970s existing building (i.e., designed for gravity loads only) according to available data of an existing school building in Lucera (FG), Italy. Specifically, no "capacity design" principles are provided, and the structure presents the typical structural weaknesses of existing buildings in Italy designed in that period according to old code provisions (i.e., "Reggio Decreto" RD 2229, 1939) and available technical guidelines (e.g., Santarella 1968), e.g., inadequate transverse reinforcement for shear and confinement, strong beam/weak column, inadequate anchorage details, lower quality of materials. Three different masonry infill walls are selected, to represent weak, medium and strong infill panels, according to Hak et al. (2012). The weak infill panel is a single-leaf masonry wall with horizontally hollowed brick; the medium infill panel is a double-leaf masonry wall with horizontally hollowed brick divided by an internal cavity; the strong infill panel is a single-leaf wall with vertically hollowed brick units. Geometrical properties of the selected infilled frames are reported in Fig. 4, while mechanical proprieties of the three typologies of infill walls are reported in Table 2.

Structural details of RC beams and columns are assumed the same for both structural configurations. The beam-column joint presents no stirrups and plain round beam bars with end-hooks. The mean concrete cylindrical strength is equal to 16 MPa and the mean steel yield stress is equal to 400 MPa. A Young's modulus of 22,850 MPa and 200,000 MPa are considered for concrete and reinforcement steel, respectively. An axial load N = 250kN acting on the columns is applied to each configuration.

4.2 Macro-modelling approaches

Parametric analysis of the seismic behaviour of infilled frames is performed considering three different macro-modelling techniques: (1) a single strut joint on the opposite corner node, (2) a single strut with rigid arms at the end sections (conceptually proposed by

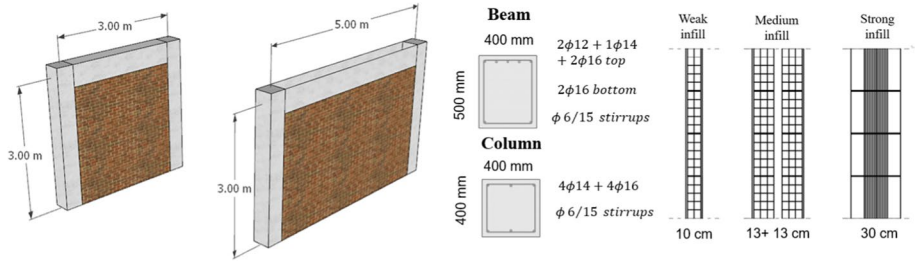

Fig. 4 Geometrical properties of the infilled frame configurations

Table 2 Mechanical proprieties of the three typologies of infill walls (Hak et al. 2012)

Typology	f_{wh} (MPa)	f_{wv} (MPa)	f_{wu} (MPa)	f_{ws} (MPa)	E_{wh} (MPa)	E_{wv} (MPa)	G (MPa)	W (kN/m^3)
Weak	1.18	2.02	0.44	0.55	991	1873	1089	6.87
Medium	1.11	1.50	0.25	0.31	991	1873	1089	6.87
Strong	1.5	3.51	0.3	0.36	1050	3240	1296	7.36

f_{wh}, Compression strength for the horizontal direction; f_{wv}, Compression strength for the vertical direction; f_{wu}, Sliding shear resistance of the mortar joints; f_{ws}, Shear resistance under diagonal compression; E_{wh}, E_{wv}, Elastic modulus of the infill in the diagonal, horizontal and vertical direction, respectively; G, Shear modulus of the infill; W, Unit weight of the infill

Pampanin, personal communication, 2002, and adopted in subsequent research works, e.g., Gentile et al. 2019c) and (3) a triple strut model. A qualitative illustration of the three selected techniques is reported in Fig. 5, where A_w is the cross-section area of the strut and z is the contact zone length, derived according to Stafford Smith (1967).

Firstly, an analytical prediction for each configuration is performed by using the Simple Lateral Mechanism Analysis (SLaMA) method (NZSEE 2017). SLaMA is an analytical mechanics-based procedure to assess the seismic performance of Reinforced Concrete (RC) and UnReinforced Masonry (URM) existing buildings. The method has been introduced and further developed as part in the New Zealand Society for Earthquake Engineering (NZSEE) "Seismic Assessment Guidelines" 2006–2017 (NZSEE 2006, 2017; Pampanin 2017) and widely adopted and validated in past studies in the literature (e.g., Del Vecchio et al. 2018; Gentile et al. 2019a, b, c, d; Bianchi et al. 2019; Pedone et al. 2022; Sansoni et al. 2022). The main step of the SLaMA procedure can be summarized as (Fig. 6): (i) assess the flexural and shear capacity (in terms of both moments/forces and rotations/

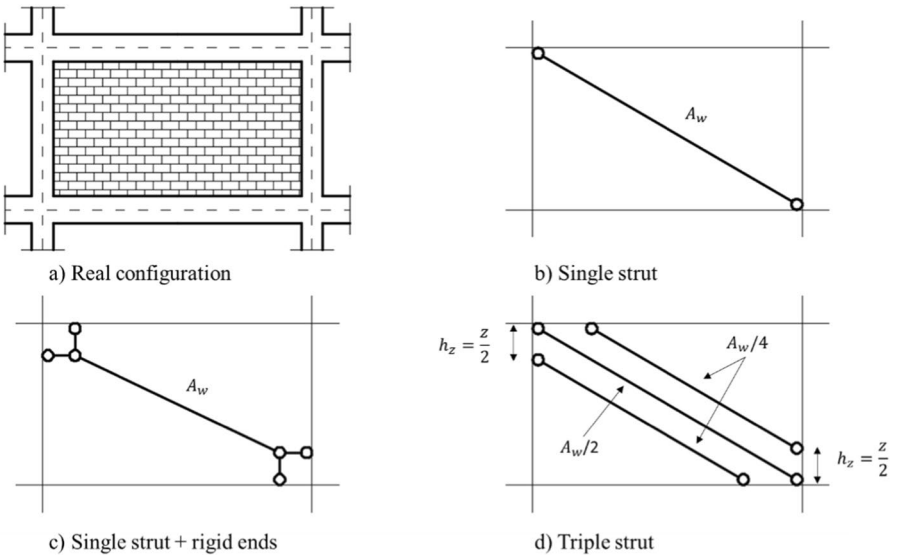

Fig. 5 Qualitative illustration of the different macro-modelling techniques adopted for parametric analysis

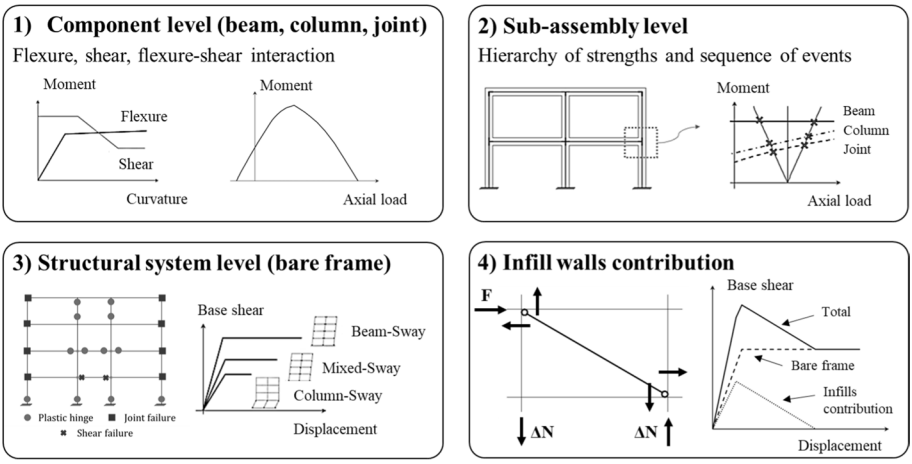

Fig. 6 Flowchart of the SLaMA method, including the influence of the infill walls in the global building response (modified after Gentile et al. 2019c)

displacements) of the structural members (i.e., beams, columns, and beam-column joints), as well as the flexural-shear and the axial load-moment (N-M) interaction diagrams; (ii) evaluate the "hierarchy of strengths" of each beam-column subassemblies by comparing the capacities of the connected structural elements in an N-M interaction diagram (Pampanin et al. 2007; Tasligedik et al. 2018); and (iii) evaluate the local failure mechanisms and the expected global inelastic mechanism of the seismic-resisting systems and, finally, the global force–displacement capacity curve.

Recently, a refinement of the SLaMA method including the influence of the infill walls in the global building response (capacity curve) has been carried out and validated by Gentile et al. (2019c, d). The SLaMA method for infilled frames (SLaMA-infill) is based on the calculation of the overturning moment and base shear contributions related to the infills and the frame, independently. Specifically, the infill panels are idealized as equivalent struts and, in order to evaluate their contribution to the global base shear, the strut forces are decomposed into their horizontal and vertical components; then, as pointed out by Gentile et al. (2019c), the overturning moment contribution provided to the infill ($OTM_{infills}$) can be calculated, similarly to the coupling contribution of the beams within the frame, considering the vertical components of the strut forces, which create tension–compression couples. Thus, the $OTM_{infills}$ can be converted into base shear $V_{b,infills}$ considering the effective height of the structure H_{eff}, according to the original SLaMA method, $V_{b,infills} = OTM_{infills}/H_{eff}$. Finally, the sum of the bare-frame and infills contributions defines the global response of the structure (Fig. 6). More details on the SLaMA-infill methodology can be found in Gentile et al. (2019c).

In this preliminary study, a refinement of the SLaMA method is proposed and adopted to compute the elastic stiffness of the bare frame capacity curve. In fact, the original SLaMA method approximates the force–displacement capacity curve of the structure through a bilinear elastic−perfectly-plastic curve. In other words, the global capacity curve is obtained by assessing the displacement related to the first attainment of the ultimate limit state (ULS) rotation or moment/shear (in case of brittle failure mechanisms) in any beam-column-joint subassembly and the base shear associated to the ultimate global inelastic

mechanism, while the base shear at the yielding point of the structure is assumed to be equal to the ultimate strength capacity. Therefore, a possible refinement to the method consists of evaluating the base shear at intermediate stages (e.g., considering different limit states), as recently suggested and implemented in Sansoni et al. (2022) for the application of the SLaMA method to URM structures (i.e., referred to as SLaMA-URM). In particular, in this work, the base shear corresponding to the achievement of the first yielding rotation of the structural element is evaluated by using an equilibrium approach at an intermediate (yielding) point similar to the one adopted for the ultimate point. Therefore, once knowing the yielding displacement of the capacity curve, the elastic stiffness of the capacity curve can be better identified. This refinement of the procedure can lead to a better evaluation of the capacity curve for infilled frames, since the typical overestimations of the base shear at yielding, due to the use of a bilinear capacity curve, are reduced.

Then, numerical nonlinear static analyses are performed for the case-study structures using the software SAP2000 (CSI 2019). Details of the adopted modelling approach are reported in Fig. 7.

Structural members are modelled by elastic components with lumped plasticity at the end sections. The plastic hinges are described using proper moment–curvature relationships and the plastic hinge length is calculated according to Priestley et al. (2007). The shear failure mechanism is also evaluated. Panel zones are modelled by rigid arms with an additional rotational spring to take into account the possible failure of beam-column joints (Pampanin et al. 2003). Specifically, the moment-rotation springs are located between beams and columns and their behaviour is described by equivalent column moment vs. drift curves, following the provisions reported in the New Zealand guidelines for seismic assessment of existing buildings (NZSEE 2017). Joint ultimate drift capacity is set equal to 1% and 1.5% for exterior and interior joints, respectively, consistently with past experimental observations and according to Pampanin et al. (2003). Equivalent strut properties are obtained according to the procedure proposed by Bertoldi et al. (1993), discussed above. Diagonal struts are modelled by a non-linear axial spring element described by a simplified tri-linear stress–strain relationship, derived from the Crisafulli hysteresis. Hence, only two parameters are needed, the strain at the peak stress ε'_w and the ultimate strain ε_u, while the ultimate stress f'_m is obtained according to Bertoldi et al. (1993). In this preliminary study, a value of $\varepsilon'_w = 0.0013$ and $\varepsilon_u = 0.0045$ are adopted, as reported in Hak et al. (2012). For the single strut approach, an additional model is also performed by using the software OpenSees (python library, Zhu et al. 2018), in order to consider an alternative description

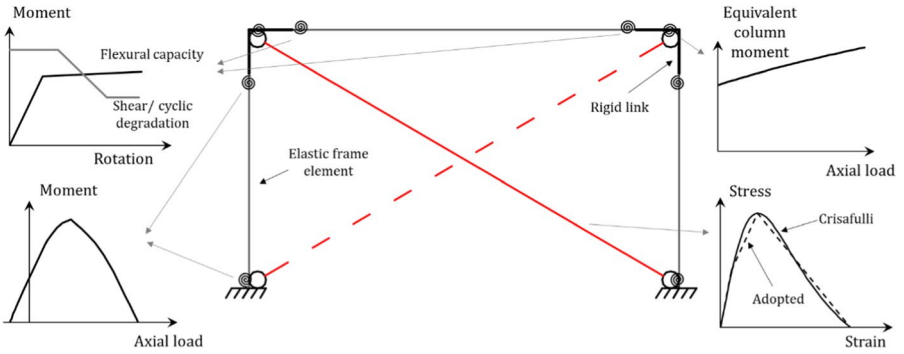

Fig. 7 Schematic illustration of the adopted numerical modelling strategy

of the infill stress–strain hysteresis. In this model, a fiber section is defined for the equivalent strut and the stress–strain law of the fibers is described by a Kent-Scott-Park concrete material (Kent and Park 1971), setting the parameters in order to best approximate the Crisafulli hysteresis, as for the previous numerical models implemented in SAP2000 (both SAP2000 and OpenSees do not include the Crisafulli hysteresis in their libraries).

4.3 Nonlinear static analyses

The obtained numerical results are presented in Fig. 8. An ultimate interstorey drift of 1.0% is assumed for all the analyses since the panel joint shows a critical damage level at this drift level (Pampanin et al. 2002).

The different macro-modelling approaches provide a very similar nonlinear global behaviour for all the considered configurations. Furthermore, the SLaMA-based approach allows predicting the seismic response of the infilled frame with good

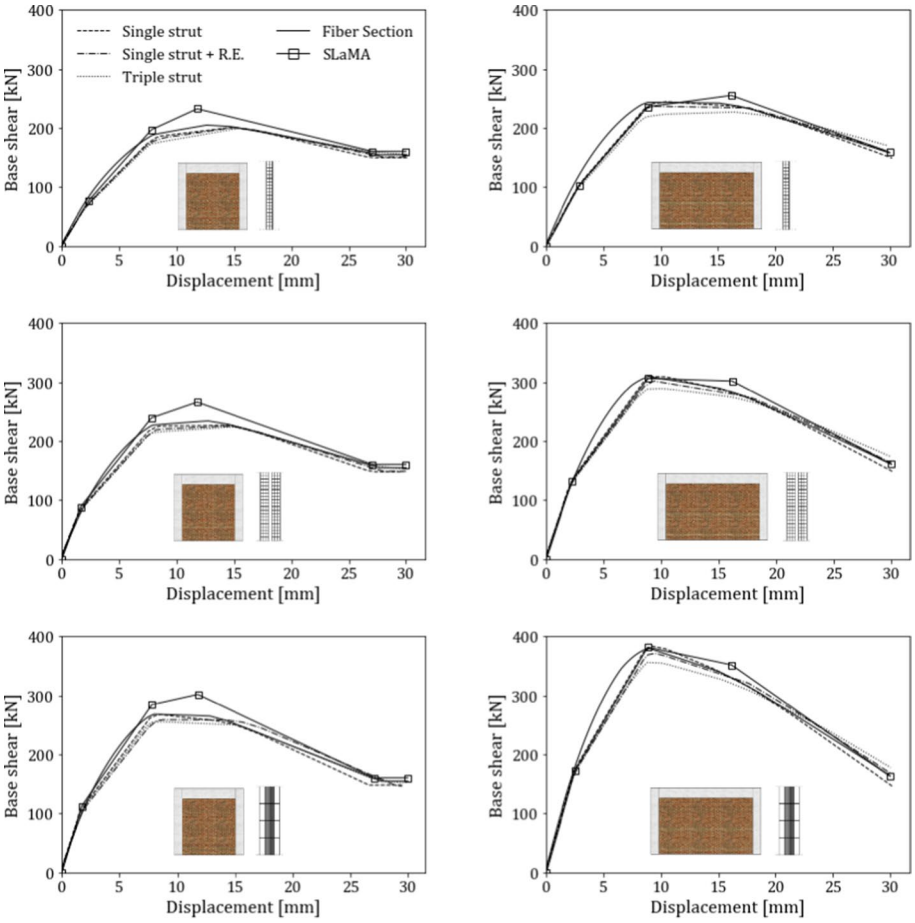

Fig. 8 Result of the parametric analysis with different macro-modelling approaches for infilled frame structures (note: R.E. = rigid ends)

accuracy. An increase in global strength is observed when considering a stronger infill panel. However, it is worth noting that this increased capacity is related to an increased level of local shear demand in the structural elements, which can result in a brittle failure mechanism.

Looking at the results of this preliminary study, it can be concluded that all the considered macro-modelling approaches (as well as the analytical SLaMA-based approach) are valuable to achieve the objectives of this paper. In the following section, the fiber section strut model (i.e., OpenSees model) will be adopted.

4.4 Numerical versus experimental results

In the previous section, preliminary parametric analyses with different macro-modelling approaches were reported, based on the adoption of the Crisafulli stress–strain relationship and fixed values for the strain parameters, according to Hak et al. (2012). However, these values were calibrated by referring to available experimental results on RC frames with weak masonry infills. Moreover, Hak et al. (2012) highlighted the need to extend the procedure to different masonry infill typologies, once relevant experimental data would be available. Hence, this section aims to calibrate strain parameters for medium and strong infills, according to experimental tests on RC infilled frame structures. To achieve this scope, the experimental tests performed by Mehrabi et al. (1996), Cavaleri and Di Trapani (2014) and Morandi et al. (2018a) are selected. Geometrical details and material properties of the infill panels are reported in Tables 3 and 4. More information about the specimens can be found in the previously cited papers.

The experimental results are compared with the numerical results developed in OpenSees. It is worth noting that, for the experimental testing performed by Mehrabi et al. (1996), the elastic modulus in the diagonal direction is assumed to be equal to the one in the vertical direction, according to Di Trapani et al. (2017), considering that the elastic modulus in the horizontal direction is not provided. Results of the implemented calibration are presented in Fig. 9.

Although out of the scope of this study, the numerical vs. experimental comparison in terms of cyclic response of the infilled frame tested by Morandi et al. (2018a) is shown in Fig. 9a. The results highlight a good agreement when considering a strain at maximum stress $\varepsilon'_m = 0.0013$ and an ultimate strain $\varepsilon_u = 20\varepsilon'_w$. The force–displacement behaviour is well captured, while the hysteretic behaviour of the numerical model slightly overestimates the energy dissipation of the infilled structure. Regarding the experimental tests performed by Cavaleri and Di Trapani (2014) and Mehrabi et al. (1996), the comparison between the backbone curve of cyclic tests and the numerical results shows a good accuracy when adopting an ultimate strain of the strut $\varepsilon_u = 10\varepsilon'_w$. Table 5 summarizes the main parameters of the equivalent strut models.

The implemented study highlights the great influence of the thickness, instead of the infill strength or stiffness, in the choice of the strain parameters during the calibration process. According to these results and considering that this section aimed to evaluate a range of strain parameters for medium and strong masonry infill types, in the next section the numerical investigation is carried out referring to values of ultimate strains ε_u equal to 10 and 20 times the peak strain ε'_w for these two categories, respectively, while a peak strain value of $\varepsilon'_w = 0.0013$ is adopted for both cases, according to the results.

Table 3 Geometrical details of the specimens tested by Morandi et al. (2018a), Cavaleri e Di Trapani (2014) and Mehrabi et al. (1996)

Author	Specimen #	Masonry typology	t_w(mm)	h(mm)	h_w(mm)	l(mm)	l_w(mm)	l/h(–)	d_w(mm)
Morandi et al. (2018a)	TA2	Clay masonry	350	3125	2950	4570	4220	1.46	5149
Cavaleri and Di Trapani (2014)	S1B	Clay masonry	150	1800	1600	1800	1600	1.00	2263
Mehrabi et al. (1996)	4	Hollow concrete	92	1540	1426	2210	2032	1.43	2482

Table 4 Mechanical properties of masonry infill walls: available data from vertical, lateral and diagonal compressive tests on masonry and compressive test on mortars

Author	f_{wh} (MPa)	f_{wv} (MPa)	f_{wu} (MPa)	f_{ws} (MPa)	E_{wh} (MPa)	E_{wv} (MPa)	G (MPa)
Morandi et al. (2018a)	1.08	4.64	0.265	–	494	5299	2120
Cavaleri and Di Trapani (2014)	4.18	8.66	–	1.07	5038	6401	2547
Mehrabi et al. (1996)	–	10.6	0.49	–	–	4596	–

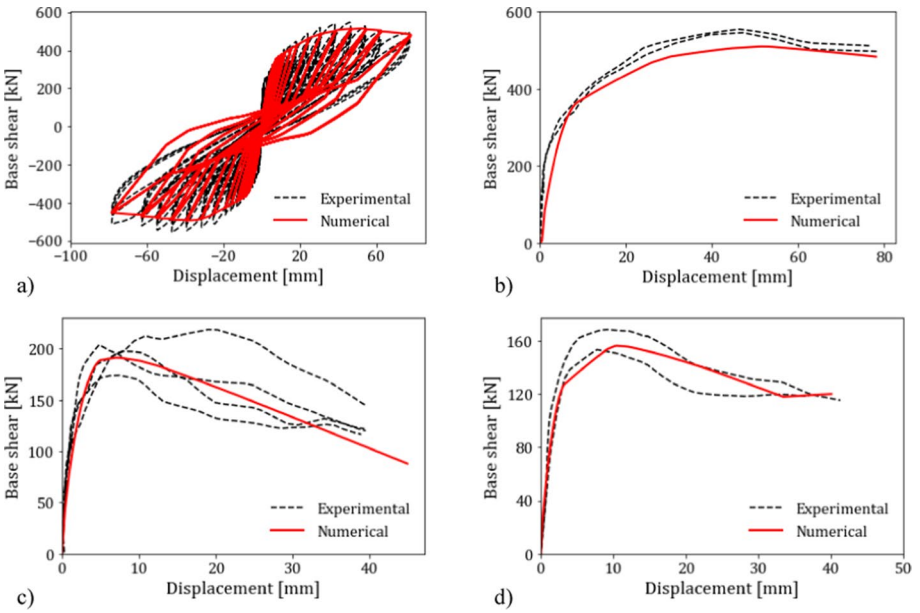

Fig. 9 Comparison between experimental and numerical results: **a** cyclic and **b** monotonic response of the infilled frame tested by Morandi et al. (2018a); monotonic response of the infilled frame tested by **c** Cavaleri and Di Trapani (2014) and **d** Mehrabi et al. (1996)

Table 5 Parameters of the equivalent strut models

Authors	$E_{w\,\theta}$ MPa	b_w/d_w –	t_w mm	f'_m MPa	P_{max} kN	ε'_w –	ε'_u –
Morandi et al. (2018a)	983.3	0.19	350	0.96	341.7	0.013	$20 \cdot \varepsilon'_w$
Cavaleri e Di Trapani (2014)	5585.9	0.13	150	4.80	218.0	0.013	$10 \cdot \varepsilon'_w$
Mehrabi et al. (1996)	4595.6	0.18	92	2.87	118.4	0.013	$10 \cdot \varepsilon'_w$

5 Shape functions of infill-frame displacement incompatibility

5.1 Case-study infilled frames and modelling approach

A parametric analysis is implemented to determine the shape functions describing the displacement incompatibility between the infill wall and RC frame. The selected case-study infilled frames are the same as the preliminary analysis (Fig. 4) developed in the previous paragraph. Moreover, different axial load values are applied to the RC columns (i.e., N = 120kN, 270kN and 420kN) to represent portal frames located at three different story levels, considering a low-rise building. According to the modelling strategies adopted, firstly, the global seismic response of each configuration is obtained by using the equivalent strut model approach. Secondly, two interstorey drift values ($\vartheta = 0.4\%$ and $\vartheta = 0.9\%$) are selected to represent Damage Limit State (DLS) and Ultimate Limit State (ULS) of the infilled frame, according to the numerical and experimental tests available in the literature (Magenes and Pampanin 2004; Hak et al. 2012; Morandi et al. 2018a). Then, a continuous bi-dimensional model is developed for each configuration and the equal secant stiffness to the equivalent strut model at each fixed interstorey drift is obtained by iteratively scaling the thickness of shell elements. Concerning the bi-dimensional model, the infill wall is modelled as a continuous element by using elastic orthotropic shell elements. Gap elements, able to transfer compression stresses only, are adopted to model the contact interface between the frame and infill. A similar modelling technique can be found in Cavaleri and Di Trapani (2015) and Doudoumis (2007). Friction phenomena are neglected in the numerical investigation due to the complexity of defining a reliable value of the friction coefficient (according to the Coulomb law, commonly used). Moreover, considering that friction progressively varies in the case of cyclic loading (Cavaleri and Di Trapani 2015) not influencing the overall system behaviour (Fiore et al. 2012), it is reasonable to neglect this contribution in a preliminary assessment of the detachment mechanism. A qualitative illustration of the bi-dimensional model is presented in Fig. 10.

Hence, detachment values are evaluated for each case study and the shape functions of the infill-frame displacement incompatibility at the fixed interstorey drifts are finally obtained. Operatively, the first step consists in assessing the horizontal and vertical displacement of the structural frame and infill panel edges. Displacement incompatibility is computed as the difference between the displacement of the frame and the displacement of the infill panel along the vertical and horizontal directions (i.e., Horizontal Displacement Incompatibilities, HDI; Vertical Displacement Incompatibilities, VDI). Thus, shape

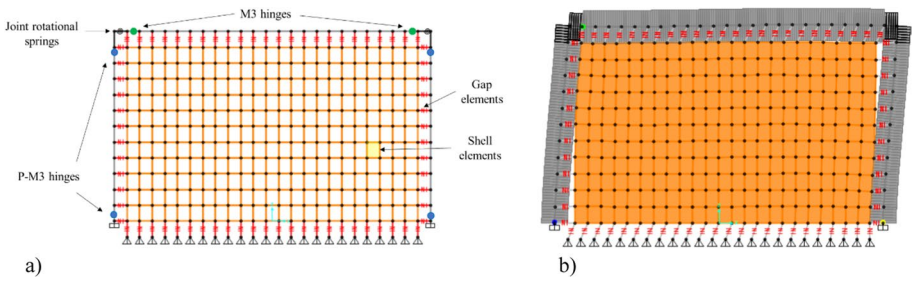

Fig. 10 **a** Schematic illustration of the continuous bi-dimensional model of the infilled frame structure; **b** example of results in terms of displacement incompatibility

functions are defined by the envelope of displacement incompatibility points, considered a normalized position along the frame.

5.2 Results and discussion

In Table 6 the details of the specimens taken into account for the parametric analysis as well as the mechanical properties of the equivalent strut models are reported, while Fig. 11 shows the results for all the infilled frames in terms of seismic performance (force–displacement capacity curves).

Results show that the axial load on columns strongly influences the strength and stiffness of the structure under seismic loads. Furthermore, the strength and stiffness of the structures also increase in the case of strong infill panels, as well as considering a longer beam span length.

The shape functions of the displacement incompatibility between the infill wall and frame are reported in Fig. 12 for the beam span length $l = 3$ m and Fig. 13 for the beam span length $l = 5$ m. Maximum detachment values in the horizontal and vertical directions are provided in Table 7, together with the observed contact length values, expressed in terms of beam/column length percentage.

As expected, displacement incompatibility increases considering higher drift values for all configurations. It can be noticed that when the beam span length increases, the seismic horizontal displacement incompatibility increases while the vertical displacement incompatibility decreases. The main differences can be found for the strong infill when compared to weak and medium infills. It is worth highlighting that, as shown in previous Table 2, strong infill walls are characterized by a higher ratio between stiffness in vertical and horizontal directions when compared to weak and medium infills. Considering $l = 3$ m, the strong infill leads to higher values of detachment in the horizontal direction (column-infill wall) and smaller values in the vertical direction (beam-infill wall) than weak and medium infills. The maximum displacement incompatibility values are recorded for the top corner of the frame. The detachment increases when considering higher values of axial load and stronger infill: strong infill with $N = 420$ kN leads to the maximum detachments $\Delta_s = 5.2$ mm for interstorey drift $\vartheta = 0.4\%$ and $\Delta_s = 11.3$ mm for $\vartheta = 0.9\%$. Generally, weak and medium infills show similar behaviour, while strong infill leads to higher values of displacement incompatibility. Moreover, the contact length has clearly an opposite trend than the detachment (i.e., it decreases when considering a stronger infill or lower axial load on columns). This behaviour is in agreement with the relationship proposed by Stafford Smith (1967). On the other hand, no significative differences in terms of contact length have been observed considering higher values of interstorey drift. Generally, the higher the interstorey drift ratio, the higher the contact length values, especially considering the beam and left column. The higher contact length values are observed for the right column-infill in the case of weak/medium infills and high axial load (N = 420kN), $\%L_{contact} = 36\%$. For the beam-infill interface, the contact length range values are 15–31%.

Considering $L = 5$ m, similar considerations can be made. Displacement incompatibility increases considering a higher value of beam span length. The maximum value of detachment is recorded at the top corner in the horizontal direction $\Delta_s = 6.9$ mm and $\Delta_s = 14.9$ mm for interstorey drift $\vartheta = 0.4\%$ and $\vartheta = 0.9\%$, respectively. Displacement incompatibility increases when considering a stronger infill panel even in this configuration. However, when considering higher axial load values, detachment decreases in most of the configurations. Main differences are noticed for the vertical detachment, especially

Table 6 Characteristics of the infilled frame specimens for parametric analysis

#	h (cm)	l (cm)	h_w (cm)	l_w (cm)	d_w (cm)	Infill type	N (kN)	$E_{w\theta}$ (MPa)	b_w/d_w (–)	t_w (mm)	f_m' (MPa)	P_{max} (kN)	ε_w'(–)	ε_u'(–)
1	300	300	275	260	378.5	Weak	120	1820.6	0.23	100	1.43	124.9	0.0013	0.0045
2	300	300	275	260	378.5	Weak	270	1820.6	0.24	100	1.39	124.9	0.0013	0.0045
3	300	300	275	260	378.5	Weak	420	1820.6	0.24	100	1.35	124.9	0.0013	0.0045
4	300	300	275	260	378.5	Medium	120	1820.6	0.18	260	1.01	183.0	0.0013	0.0130
5	300	300	275	260	378.5	Medium	270	1820.6	0.19	260	0.99	183.0	0.0013	0.0130
6	300	300	275	260	378.5	Medium	420	1820.6	0.19	260	0.98	183.0	0.0013	0.0130
7	300	300	275	260	378.5	Strong	120	2175.1	0.17	300	1.27	245.2	0.0013	0.0260
8	300	300	275	260	378.5	Strong	270	2175.1	0.17	300	1.24	245.2	0.0013	0.0260
9	300	300	275	260	378.5	Strong	420	2175.1	0.18	300	1.22	245.2	0.0013	0.0260
10	300	500	275	460	535.9	Weak	120	1386.3	0.27	100	1.23	176.9	0.0013	0.0045
11	300	500	275	460	535.9	Weak	270	1386.3	0.28	100	1.18	176.9	0.0013	0.0045
12	300	500	275	460	535.9	Weak	420	1386.3	0.29	100	1.15	176.9	0.0013	0.0045
13	300	500	275	460	535.9	Medium	120	1386.3	0.20	260	0.92	259.2	0.0013	0.0130
14	300	500	275	460	535.9	Medium	270	1386.3	0.21	260	0.90	259.2	0.0013	0.0130
15	300	500	275	460	535.9	Medium	420	1386.3	0.21	260	0.89	259.2	0.0013	0.0130
16	300	500	275	460	535.9	Strong	120	1506.0	0.19	300	1.13	347.3	0.0013	0.0260
17	300	500	275	460	535.9	Strong	270	1506.0	0.20	300	1.11	347.3	0.0013	0.0260
18	300	500	275	460	535.9	Strong	420	1506.0	0.20	300	1.09	347.3	0.0013	0.0260

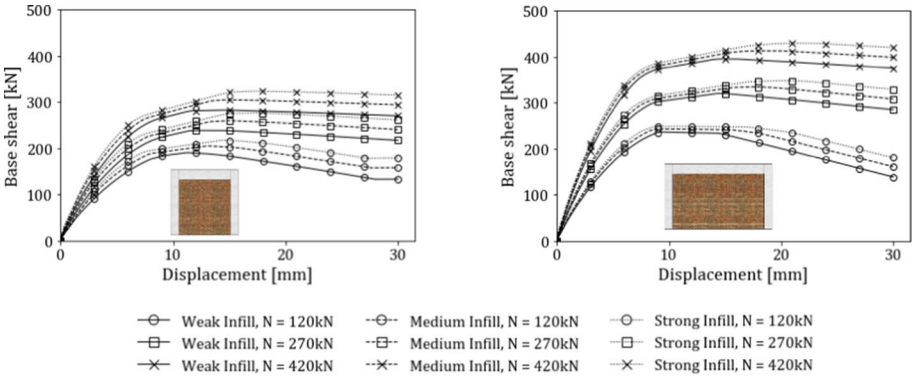

Fig. 11 Capacity curves of the infilled frame structure for each configuration

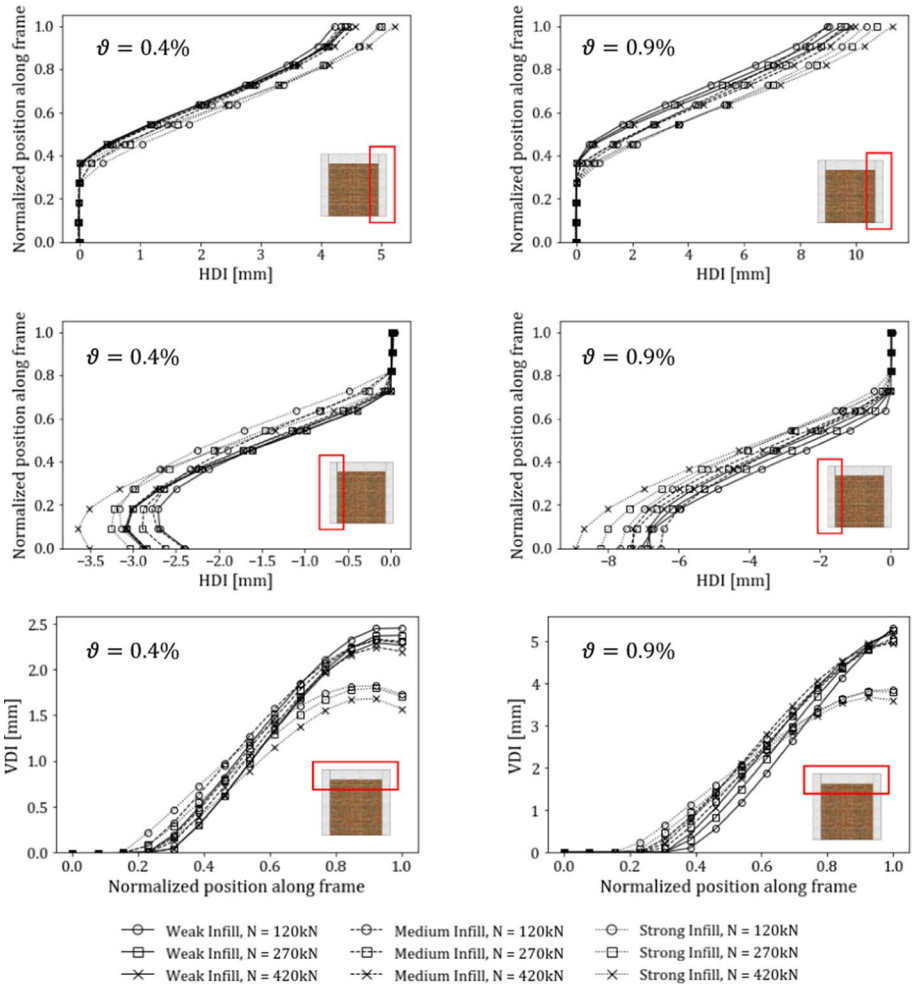

Fig. 12 Shape functions of Horizontal and Vertical Displacement Incompatibilities (HDI, VDI) between masonry infill wall and frame structure for 3 m beam span length

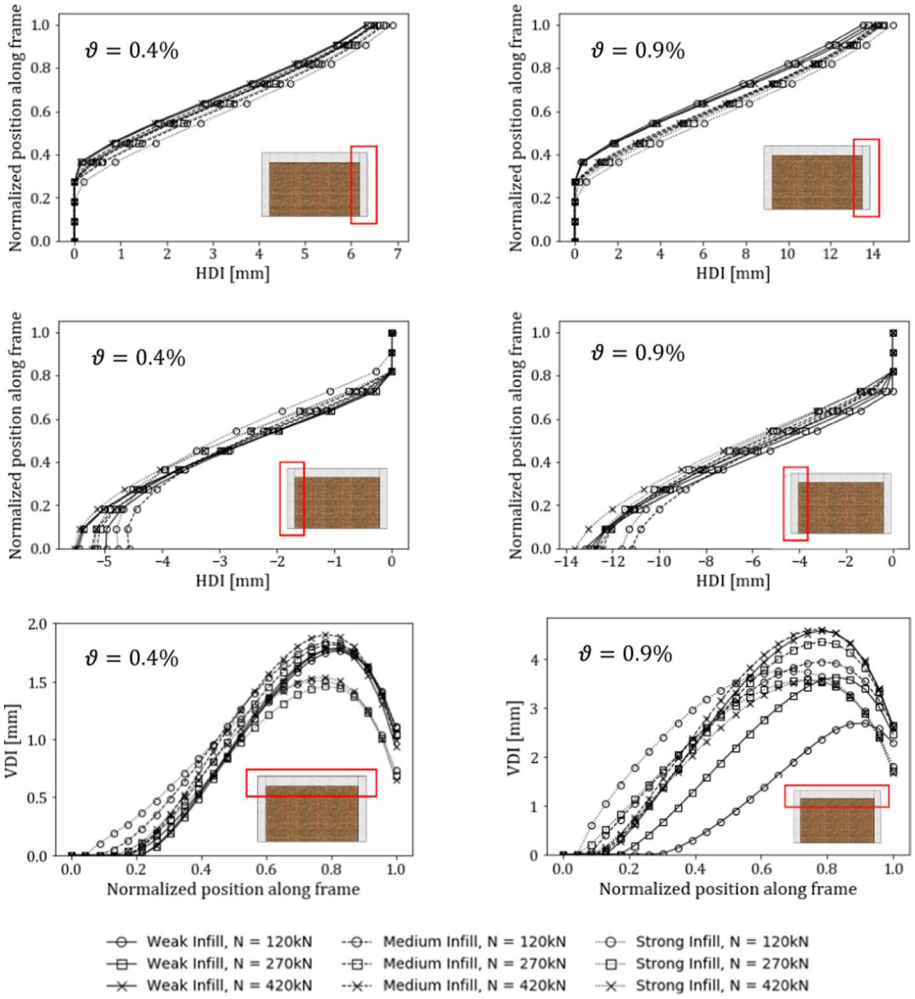

Fig. 13 Shape functions of Horizontal and Vertical Displacement Incompatibilities (HDI, VDI) between masonry infill wall and frame structure for 5 m beam span length

for $\vartheta = 0.9\%$ since the plastic hinges sequence of the structural frame significantly influences the displacement incompatibility between beam and infill wall. It is highlighted that in this study a pre-seismic-code frame structure is considered and that the failure mode is a mixed sidesway mechanism (i.e., lack of capacity design principles). Increasing the axial load on columns leads to a higher capacity of the panel zone, so when $N = 420$ kN plastic hinge occurs on the beam for a positive bending moment, while when $N = 120$ kN shear failure of the panel zone occurs. Furthermore, the residual strength of the infill wall may modify the bending moments in the beam leading to different shape behaviour. For these reasons, it is not easy to identify a common behaviour for VDI. However, it is observed that vertical displacement incompatibility values are always smaller than horizontal ones and thus of lesser interest. It is interesting to notice that the configuration with strong infill and $N = 120$ kN shows shape functions significantly different from the others, since both

Table 7 Maximum displacement incompatibility values

Spec	h	l	Infill type	N	Δ_{DI} ($\vartheta = 0.4\%$) (mm)			Δ_{DI} ($\vartheta = 0.9\%$) (mm)			$\%L_{contact}$ ($\vartheta = 0.4\%$) (–)			$\%L_{contact}$ ($\vartheta = 0.9\%$)(–)		
#	mm	mm	–	kN	Col_{sx}	Beam	Col_{dx}	Col_{sx}	Beam	Col_{dx}	Col_{sx} (%)	Beam (%)	Col_{dx} (%)	Col_{sx} (%)	Beam (%)	Col_{dx} (%)
1	3000	3000	Weak	120	−2.7	2.5	4.2	−7.1	5.3	9.0	27	23	36	27	31	36
2	3000	3000	Weak	270	−3.1	2.4	4.4	−6.9	5.2	9.5	27	31	36	27	31	36
3	3000	3000	Weak	420	−3.1	2.3	4.5	−6.9	5.2	9.8	27	31	36	27	31	36
4	3000	3000	Medium	120	−2.8	2.3	4.3	−6.5	5.1	9.0	18	15	27	18	23	27
5	3000	3000	Medium	270	−2.9	2.3	4.4	−7.4	5.0	9.6	18	23	36	27	23	27
6	3000	3000	Medium	420	−3.1	2.2	4.6	−7.3	4.9	10.0	27	23	36	27	23	27
7	3000	3000	Strong	120	−3.2	1.8	5.0	−7.7	3.8	10.4	18	15	27	18	15	27
8	3000	3000	Strong	270	−3.2	1.8	5.0	−8.2	3.8	10.8	18	15	27	18	15	27
9	3000	3000	Strong	420	−3.6	1.7	5.2	−8.9	3.7	11.3	18	23	27	18	23	27
10	3000	5000	Weak	120	−5.0	1.8	6.5	−13.2	2.7	13.5	18	22	27	27	30	27
11	3000	5000	Weak	270	−5.4	1.8	6.4	−13.0	3.6	13.8	18	22	27	18	17	27
12	3000	5000	Weak	420	−5.5	1.8	6.3	−12.7	4.6	14.0	18	22	27	18	13	27
13	3000	5000	Medium	120	−4.6	1.8	6.7	−11.2	3.9	14.4	18	13	27	18	4	18
14	3000	5000	Medium	270	−5.1	1.8	6.5	−12.6	4.4	14.2	18	17	27	18	9	27
15	3000	5000	Medium	420	−5.2	1.9	6.5	−12.4	4.6	14.3	18	17	27	18	9	27
16	3000	5000	Strong	120	−4.8	1.5	6.9	−11.6	3.8	14.9	9	4	18	18	4	18
17	3000	5000	Strong	270	−5.2	1.5	6.7	−12.8	3.6	14.5	18	17	27	18	4	18
18	3000	5000	Strong	420	−5.5	1.5	6.5	−13.6	3.6	14.1	18	17	27	18	9	27

Col_{sx}, Left column; Col_{dx}, Right column; Δ_{DI}, Maximum detachment values; ϑ, Interstorey drift ratio; $\%L_{contact}$, Contact zone length expressed in beam/column length percentage

the joint panels achieve the failure and the residual strength of infill modifies the bending moment in the beam. Concerning the contact length, similarly to the L = 3 m configuration, it decreases in the case of a stronger/stiffer infill or lower axial load on columns. Generally, the L = 5 m configurations lead to lower values of contact length with respect to the L = 3 m configurations. Even in this case, for the infill-column contact length, no significative differences are observed considering higher values of interstory drift ratio (e.g., $\%L_{contact} = 18–27\%$ for right column-infill). On the other hand, the interstory drift value strongly affects the contact/detachment between infill and beam, leading to lower contact length values if higher drift values are considered. For the beam-infill interface, lower contact length values are obtained when considering higher drift values ($\vartheta = 0.9\%$), lower axial load, and strong infill, $\%L_{contact} = 4\%$; once again, this result is associated to shear failure of the joint panels, as previously discussed.

6 Design of structural and energy retrofitting construction details

Improving the overall performance of the building envelope (facade) represents a crucial aspect to enhance seismic safety and energy efficiency of existing buildings. However, generally, local displacement incompatibility issues are not directly considered because of the lack of a standardized and easy-to-apply procedure to assess local infill-frame interaction. The proposed concept of shape functions, as well as the modelling approach adopted in this paper, may be used to design construction details for both seismic and energy retrofit solutions in view of an integrated intervention. A possible operative flowchart for the design of construction details of both seismic and energy retrofit solutions for an integrated requalification of RC buildings is reported in Fig. 14.

The methodology presented in this paper can be used for any infilled frame configuration in order to derive shape functions of displacement incompatibility without performing

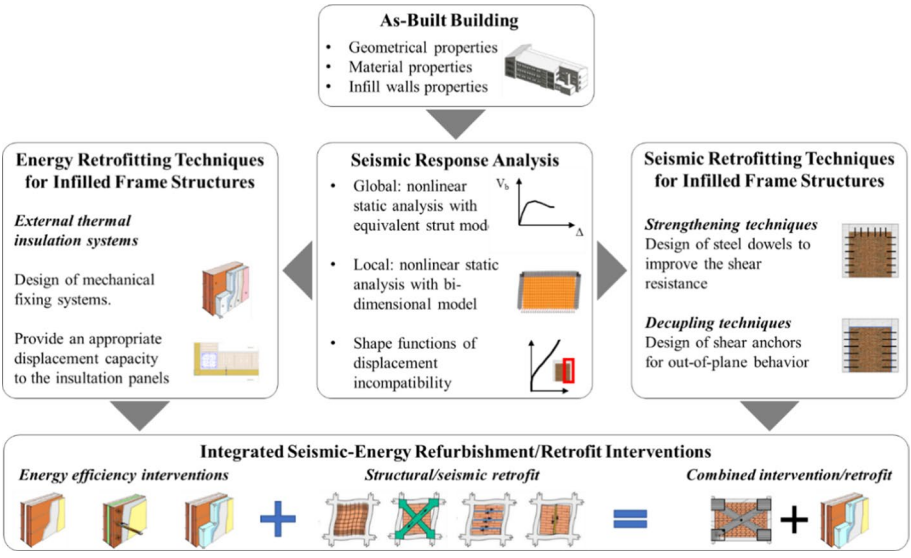

Fig. 14 Conceptually flow-chart for the design of integrated seismic-energy retrofit interventions using the proposed concept of displacement incompatibility shape functions

a more complex nonlinear FEM (micro-model) analysis. Alternatively, as a preliminary step, the most similar configuration among those reported in this work can be adopted and built on. By assessing the expected values and shape of detachment at the infill-frame interface, appropriate structural details can be designed for either strengthening or decoupling approaches and techniques. When considering decupling techniques, shape functions can be used to identify the best location for shear anchors (i.e., contact zones) and to design their length to guarantee their effectiveness. Clearly, in the case of decoupling techniques, shear anchors should be designed and detailed to only prevent out-of-plane failure mechanisms of the panel, thus in-plane load transfer between the infill and frame should be avoided. Milanesi et al. (2018b) pointed out that the use of steel ribbed rebars as infill-frame connections to increase the out-of-plane capacity of the panel could not allow for in-plane differential movements between the infill and the surrounding frames, consequently leading to damage to the blocks in which the rebars are located. Therefore, it is suggested to use anchors/rebars not fully embedded in the masonry units to avoid possible local interaction. In that direction, some possible solutions to avoid stress concentrations in the blocks may include the use of shear anchors placed in the columns and in a side opening of the block filled with elastomer to allow for in-plane movements, as experimentally investigated by Marinković and Butenweg (2022) (Fig. 15a). Moreover, other decoupling solutions for infilled frame structures in which the OOP capacity is provided by specific infill-frame connection, based on ad-hoc shear keys, have been presented (e.g., Preti et al. 2015; Morandi et al. 2018b). As an example, in the decoupling solution investigated by Morandi et al. (2018b), steel shear keys connected to the columns are provided and the masonry units at the infill-column interface are C-shaped to accommodate the shear key (Fig. 15b). In view of the implementation of this type of construction detail, the proposed concept of shape functions of displacement incompatibility may provide useful information to adequately design the geometrical dimension of the shear keys and the C-shaped blocks.

Otherwise, considering strengthening solutions, steel dowels are typically adopted to improve the shear resistance at the interface and avoid detachments. In this case, shape functions allow to identify the location and value of the maximum detachment at the interface and therefore the expected most stressed dowel. A step-by-step design/worked

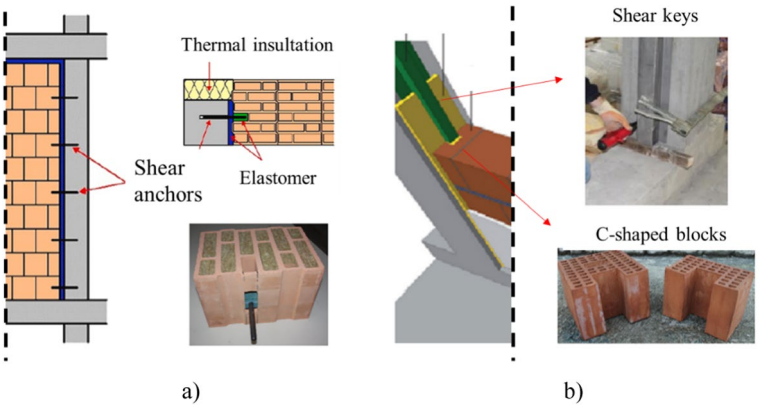

Fig. 15 Examples of construction details to avoid out-of-plane failure in the case of decoupling retrofit techniques: **a** shear anchors (modified after Marinković and Butenweg 2022); **b** shear keys with C-shaped masonry blocks (modified after Morandi et al. 2018b)

example of shear dowels in strengthening retrofit techniques according to the herein proposed displacement incompatibility shape function methodology is provided in the "Appendix". Finally, it is recommended to adequately design the connection between bare structure and energy efficiency rehabilitation solutions, as in the case of external thermal insulation systems, to allow for an adequate relative displacement movement and avoid possible local stress concentration and failure of the new high-performance envelope panel. In such a case, the required displacement capacity can be evaluated by using the proposed concept of shape functions. Specifically, a practical and efficient solution could rely upon mechanically fixed connection systems (rather than glued-on solutions), with a specifically designed displacement capacity for the critical insulation panels (i.e., those panel units located at the infill-frame interface).

7 Conclusions

In this paper, a methodology to assess the seismic displacement incompatibility between RC frame and masonry infill panel based on the concept of shape functions has been presented. Parametric analyses of different infilled frame configurations have been performed to investigate the key parameters affecting displacement incompatibility and provide a preliminary range of detachment values as well as identify the maximum detachment location along the surrounding frame.

Firstly, a comparison between the seismic response of infilled frames obtained by adopting different macro-modelling techniques has been carried out. This study highlights that all the considered models provide very similar global non-linear force–displacement behaviour and are in good agreement with the experimental response available in the literature. Then, a more refined model where the infill wall is idealized using shell elements has been prepared and displacement-incompatibilities shape functions between the infill wall and frame at fixed interstorey drift have been developed. Nonlinear behaviour of shell elements has been obtained by iteratively scaling their thickness, hence equating the secant stiffness of the continuous bi-dimensional shell-element model and that of the equivalent strut model. This simplified approach allows to capture and assess the local displacement incompatibility issues without performing a more complex nonlinear micro-model. Results demonstrate that the aspect ratio of infilled frame structures strongly affects the infill-frame detachment. Moreover, it is highlighted that horizontal displacement incompatibility (i.e., infill-to-columns) is generally more severe than vertical displacement incompatibility (i.e., infill-to-beam).

The proposed concept of shape functions can be used to design structural details, such as shear keys and/or steel dowels, in view of either decoupling or strengthening retrofit strategies, in order to guarantee their effectiveness and avoid possible local failure. On the other hand, infill-frame detachment can lead to damage to energy retrofit solutions such as external thermal insulation systems, so also these techniques should be designed to provide an appropriate displacement capacity.

In this paper, structural configurations representative of existing RC frame buildings (i.e., designed to resist vertical loads only) have been selected, however, a wider class of infilled frame structures can be used to improve the study, including newly designed RC infilled frame structures. Furthermore, an extensive experimental program as well as more refined numerical investigations, based on micro-modelling approaches, would be useful to gain a better understanding of infill-frame displacement incompatibility. Finally,

the proposed study could be extended to different infill typologies. Further advancements would include the development of tables and/or analytical formulations to simply and quickly derive shape functions starting from the geometry and material properties of the infilled frame structure. Finally, it is worth noting that when beam plastic hinges are developed, the "beam elongation" effects may increase the infill-frame horizontal detachment. Future numerical/experimental investigations are needed to achieve a comprehensive understanding of this topic.

Appendix: worked example

This appendix illustrates a worked example of the possible application of the herein proposed displacement incompatibility shape functions for the design of shear dowels in strengthening retrofit techniques. This typology of retrofit techniques has been widely investigated in the past (e.g., Koutromanos et al. 2013; Facconi and Minelli 2020), as well as the use of shear dowels for the connection between infill and surrounding frames, especially for frames with RC infills (Sugano 1996; Altin et al. 2008; Moretti et al. 2014). For the latter, some provisions on the embedment length, minimum spacing of dowel bars, and minimum edge distance have been also included in international codes and guidelines (e.g., ASCE/SEI 41-17 2017; EOTA 2019).

In this application, the strengthening solution reported in Facconi and Minelli (2020) is considered, based on the use of thin glass fiber mesh reinforced mortar overlays for strengthening RC weak infilled frames. In this retrofit technique, the relative shear sliding between the masonry panel and the frame is reduced using steel dowel connections (Fig. 16). According to the authors, this investigated retrofitting solution may represent a feasible alternative for low-rise RC frame buildings located in low-to-moderate seismicity areas.

The dowels consist of a plain round steel bar (diameter $d_{dow} = 16$ mm) with nominal yield strength $f_y = 235$ MPa. In order to implement the solution as a retrofit technique suitable for practical applications, each dowel is hammered into a pre-drilled hole located in the RC frame and is located in a "pocket" into the masonry brick; the

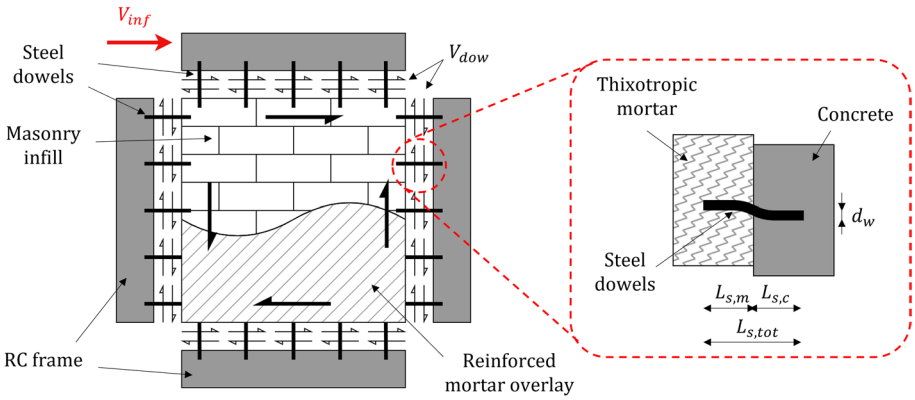

Fig. 16 Schematic illustration of steel dowel connections between the masonry panel and the frame (after Facconi and Minelli 2020)

Table 8 Formulations for design shear dowels length according to Gelfi et al. (2002)

$L_{dow} \geq L_{s,c} + L_{s,m} + 2d_{dow}$	$L_{s,c} = L'_{s,c} + L''_{s,c}$
$L'_{s,c} = \frac{d_{dow}}{1+\alpha_s}\sqrt{\frac{2f_y(1+\alpha_s)}{3f_{hc,con}}}$	$L''_{s,c} = d_{dow}\sqrt{\frac{2f_y}{3f_{hc,con}}}$
$L_{s,m} = \frac{L'_{s,c}}{\beta_s} + \frac{L''_{s,c}}{\sqrt{\beta_s}}$	$\beta_s = \frac{f_{c,thix}}{f_{c,con}} = \frac{1}{\alpha_s}$

L_{dow}, Dowel length; $L_{s,c}$, Embedment length in concrete; $L_{s,m}$, Embedment length in mortar; d_{dow}, Dowel diameter; $f_{c,con(thix)}$, Mean cylindrical compressive strength of concrete (thixotropic mortar); $f_{hc,con}$, Crushing strength of concrete around the dowel

Table 9 Design example of dowel length according to Gelfi et al. (2002)

α_s	β_s	$L_{s,c}'$	$L_{s,c}''$	$L_{s,c}$	$L_{s,m}$	$L_{dow,min}$
–	–	mm	mm	mm	mm	mm
0.27	3.75	22.2	25.0	47.3	18.9	98.13

pockets are thus filled with a thixotropic mortar. More details are available in Facconi and Minelli (2020). Conceptually, this solution could be applied to any typology of infills; however, due to the need to realize pockets into the bricks located at the infill-frame interface for the steel dowels, masonry infills with hollowed brick may be deemed as more suitable for its practical implementation.

Firstly, the model proposed by Gelfi et al. (2002) is adopted to design steel dowels length. This model allows to prevent failure mechanisms governed by crushing of both concrete and mortar. The whole formulations are reported in Table 8.

A design example is reported for all the infilled frames analyzed in the previous sections, considering a thixotropic mortar with mean cylindrical compressive strength of $f_{c,thix} = 60$ MPa. The obtained minimum dowel length $L_{dow,min}$ according to Gelfi et al. (2002) is reported in Table 9.

The proposed concept of displacement incompatibility shape function can be thus adopted to prevent dowel failure due to infill-frame detachment. Specifically, detachment values evaluated considering the as-built configuration can be assumed, in a conservative way, as displacement/strain demand for the dowels. The minimum lengths of the dowels placed in beams and columns for all the analyzed configurations are evaluated (Table 10) considering an interstorey drift of 0.4% and an ultimate dowel strain of 6%. It is worth mentioning that the drift value to be considered in the analyses should be a design choice, in line with the philosophy of performance-based design/retrofit. Since strengthening retrofit techniques for infilled frames cannot typically provide an enhancement of the ductility capacity of the structure (unless a selective weakening intervention is applied, in order to develop a low-damage infill system, Tasligedik and Pampanin 2017), these retrofit interventions should rather be designed in order to reduce the displacement for the design earthquake by increasing the strength/stiffness capacity of the structure. Therefore, in view of a retrofit strategy aiming to prevent the infill wall failure by limiting the displacement demand, a drift value equal to 0.4% is herein selected for the design of the shear dowels for illustrative purposes. Clearly, other design choices can be made according to the specific needs of the project.

Table 10 Minimum dowel length evaluated using the maximum expected detachment values for all the configurations

Spec	h	l	Infill type	N	Infill-frame detachment (mm)		$L_{min,beam}$	$L_{min,col}$
#	mm	mm	–	kN	Beam	Column	mm	mm
1	3000	3000	Weak	120	2.5	4.2	41.7	70.0
2	3000	3000	Medium	120	2.4	4.4	40.0	73.3
3	3000	3000	Strong	120	2.3	4.5	38.3	75.0
4	3000	3000	Weak	270	2.3	4.3	38.3	71.7
5	3000	3000	Medium	270	2.3	4.4	38.3	73.3
6	3000	3000	Strong	270	2.2	4.6	36.7	76.7
7	3000	3000	Weak	420	1.8	5	30.0	83.3
8	3000	3000	Medium	420	1.8	5	30.0	83.3
9	3000	3000	Strong	420	1.7	5.2	28.3	86.7
10	3000	5000	Weak	120	1.8	6.5	30.0	108.3
11	3000	5000	Medium	120	1.8	6.4	30.0	106.7
12	3000	5000	Strong	120	1.8	6.3	30.0	105.0
13	3000	5000	Weak	270	1.8	6.7	30.0	111.7
14	3000	5000	Medium	270	1.8	6.5	30.0	108.3
15	3000	5000	Strong	270	1.9	6.5	31.7	108.3
16	3000	5000	Weak	420	1.5	6.9	25.0	115.0
17	3000	5000	Medium	420	1.5	6.7	25.0	111.7
18	3000	5000	Strong	420	1.5	6.5	25.0	108.3

Results highlight that the proposed concept of shape functions would suggest increasing the length of the dowels located at the infill-to-column interface for all the 5 m-bay frame configurations. On the other hand, for the dowels located at the infill-to-beam interface, the expected (vertical) detachment value is less severe, and the dowel length designed according to Gelfi et al. (2002) already allows to protect the dowel failure. It is worth noting that in the retrofitted configuration, a less severe displacement incompatibility than in the as-build configuration is expected. Therefore, the proposed displacement-compatible design check should be considered as a conservative hypothesis in a preliminary design. Further research efforts are needed to develop operative design guidelines including suggestions for amended construction details based on the concept of displacement incompatibility shape functions.

Acknowledgements The authors are very grateful to Dr Simona Bianchi (TU Delft) for her constructive comments and internal revision of an earlier version of this work. The authors also acknowledge the financial support of the Italian Ministry of University and Research (MUR) for funding the Doctoral Scholarship of Livio Pedone.

Author contributions LP: conceptualization, investigation, formal analysis, writing-original draft, visualization. SP: conceptualization, supervision, project administration, writing-review and editing.

Funding Open access funding provided by Università degli Studi di Roma La Sapienza within the CRUI-CARE Agreement. The authors acknowledge the financial support of the Italian Ministry of University and Research (MUR) for funding the Doctoral Scholarship of Livio Pedone.

Data availability Some or all data, models, or code that support the findings of this study are available from the corresponding author upon reasonable request.

Declarations

Conflict of interest The authors have no relevant financial or non-financial interests to disclose.

Consent to publication All the authors agreed to submit this manuscript.

References

Altin S, Anil Ö, Kara ME (2008) Strengthening of RC nonductile frames with RC infills: an experimental study. Cem Concr Compos 30:612–621. https://doi.org/10.1016/j.cemconcomp.2007.07.003

ASCE/SEI 41-17 (2017) Seismic evaluation and retrofit of existing buildings. American Society of Civil Engineers, Reston

Bertoldi SH, Decanini LD, Gavarini C (1993) Telai tamponati soggetti ad azione sismica, un modello semplificato: confronto sperimentale e numeric (in Italian). In: Proceedings of the VI confernece on earthquake engineering in Italy. ANIDIS, Perugia

Bianchi S, Ciurlanti J, Pampanin S (2019) A SLaMA-based analytical procedure for the cost/performance-based evaluation of buildings. In: Proceedings of the 7th ECCOMAS thematic conference on computational methods in structural dynamics and earthquake engineering. COMPDYN, Crete, Greece, pp 5028–5040

Bournas DA (2018) Concurrent seismic and energy retrofitting of RC and masonry building envelopes using inorganic textile-based composites with insulation materials: a new concept. Compos Part B Eng 148:166–179. https://doi.org/10.1016/j.compositesb.2018.04.002

Brodsky A, Rabinovitch O, Yankelevsky DZ (2018) Determination of the interaction between a masonry wall and a confining frame. Eng Struct 167:214–226. https://doi.org/10.1016/j.engstruct.2018.04.001

Calvi GM, Bolognini D (2001) Seismic response of reinforced concrete frames infilled with weakly reinforced masonry panels. J Earthq Eng 5:153–185. https://doi.org/10.1080/13632460109350390

Calvi GM, Sousa L, Ruggeri C (2016) Energy efficiency and seismic resilience: a common approach. In: Gardoni P, LaFave J (eds) Multi-hazard Approaches to civil infrastructure engineering. Springer, Cham, pp 165–208. https://doi.org/10.1007/978-3-319-29713-2_9

Cardone D, Perrone G (2017) Damage and loss assessment of pre-70 RC frame buildings with FEMA P-58. J Earthq Eng 21(1):23–61. https://doi.org/10.1080/13632469.2016.1149893

Cavaleri L, Di Trapani F (2014) Cyclic response of masonry infilled RC frames: experimental results and simplified modeling. Soil Dyn Earthq Eng 65:224–242. https://doi.org/10.1016/j.soildyn.2014.06.016

Cavaleri L, Di Trapani F (2015) Prediction of the Additional Shear Action on Frame Members Due to Infills. Bull Earthq Eng 13(5):1425–1454. https://doi.org/10.1007/s10518-014-9668-z

Cavaleri L, Zizzo M, Asteris PG (2020) Residual out-of-plane capacity of infills damaged by in-plane cyclic loads. Eng Struct 209:109957. https://doi.org/10.1016/j.engstruct.2019.109957

Chrysostomou CZ, Gergely P, Abel JF (2002) A six-strut model for nonlinear dynamic analysis of steel infilled frames. Int J Struct Stab Dyn 2(3):335–353

Crisafulli FJ (1997) Seismic behaviour of reinforced concrete structures with masonry infills. PhD thesis, University of Canterbury, Christchurch, New Zealand.

Crisafulli FJ, Carr AJ (2007) Proposed macro-model for the analysis of infilled frame structures. Bull N Z Soc Earthq Eng 40(2):69–77

Crisafulli FJ, Carr AJ, Park R (2000) Analytical modelling of infilled frame structures—a general review. Bull N Z Soc Earthq Eng 33(1):30–47

CSI (2019) SAP2000 integrated software for structural analysis and design. Computers and Structures Inc

Decanini LD, Fantin GE (1987) Modelos simplificados de la mampostería incluida en porticos. Características de rigidez y resistencia lateral en astado límite. Jornadas Argentinas de Ingeniería Estructural III, vol 2, Asociacion de Ingenieros Estructurales, Buenos Aires, Argentina, pp 817–836

Del Vecchio C, Gentile R, Di Ludovico M, Uva G, Pampanin S (2018) Implementation and validation of the simple lateral mechanism analysis (SLaMA) for the seismic performance assessment of a damaged case study building. J Earthq Eng 17:1–32. https://doi.org/10.1080/13632469.2018.1483278

Di Domenico M, Ricci P, Verderame GM (2019) Experimental assessment of the out-of-plane strength of URM infill walls with different slenderness and boundary conditions. Bull Earthq Eng 17:3959–3993. https://doi.org/10.1007/s10518-019-00604-5

Di Trapani F, Cavaleri L, Bertagnoli G, Mancini G, Gino G, Malavisi M (2017) Definition of a fiber macro-model for nonlinear analysis of infilled frames. In: Proceedings of the 6th international conference on computational methods in structural dynamics and earthquake engineering, COMPDYN, Rhodes Island, Greece. https://doi.org/10.7712/120117.5645.18525

Di Trapani F, Shing PB, Cavaleri L (2018) Macroelement model for in-plane and out-of-plane responses of masonry infills in frame structures. J Struct Eng 144(2):04017198. https://doi.org/10.1061/(asce)st.1943-541x.0001926

Di Vece D, Pampanin S (2019) Combined retrofit solutions for seismic resilience and energy efficiency of reinforced concrete residential buildings with infill walls. In: Proceedings of the 14th conference on earthquake engineering in Italy. ANIDIS, Ascoli Piceno

Directive (EU) 2018/844 (2018) Directive (Eu) 2018/844 of the European Parliament and of the Council of 30 May 2018 Amending Directive 2010/31/Eu on the Energy Performance of Buildings and Directive 2012/27/Eu on Energy Efficiency. European Parliament and Council

Donà M, Minotto M, Verlato N, da Porto F (2022) A new macro-model to analyse the combined in-plane/out-of-plane behaviour of unreinforced and strengthened infill walls. Eng Struct. https://doi.org/10.1016/j.engstruct.2021.113487

Doudoumis IN (2007) Finite element modelling and investigation of the behaviour of elastic infilled frames under monotonic loading. Eng Struct 29(6):1004–10241

El-Dakhakhni WW, Elgaaly M, Hamid AA (2003) Three-strut model for concrete masonry-infilled frames. J Struct Eng 129(2):177–185

EOTA (2019) Design of structural joints with shear dowels. Technical Report (TR) 065. European Organisation for Technical Assessment, Brussels, Belgium

Facconi L, Minelli F (2020) Retrofitting RC infills by a glass fiber mesh reinforced overlay and steel dowels: experimental and numerical study. Constr Build Mater 231:117133. https://doi.org/10.1016/j.conbuildmat.2019.117133

FEMA 306 (1998) Evaluation of earthquake damaged concrete and masonry wall buildings: basic procedures manual. Federal Emergency Management Agency, Washington, DC

Fenwick RC, Megget LM (1993) Elongation and load deflection characteristics of reinforced concrete members containing plastic hinges. Bull N Z Soc Earthq Eng 26(1):28–41

Fiore A, Netti A, Monaco P (2012) The influence of masonry infill on the seismic behaviour of RC frame buildings. Eng Struct 44:133–145. https://doi.org/10.1016/j.engstruct.2012.05.023

Furtado A, Rodrigues H, Arêde A, Varum H (2016) Experimental evaluation of out-of-plane capacity of masonry infill walls. Eng Struct 111:48–63. https://doi.org/10.1016/j.engstruct.2015.12.013

Gelfi P, Giuriani E, Marini A (2002) Stud shear connection design for composite concrete slab and wood beams. J Struct Eng 128:1544–1550. https://doi.org/10.1061/(asce)0733-9445(2002)128:12(1544)

Gentile R, Del Vecchio C, Pampanin S, Raffaele D, Uva G (2019a) Refinement and validation of the simple lateral mechanism analysis (SLaMA) procedure for RC frames. J Earthq Eng. https://doi.org/10.1080/13632469.2018.1560377

Gentile R, Pampanin S, Raffaele D, Uva G (2019b) Analytical seismic assessment of RC dual wall/frame systems using SLaMA: proposal and validation. Eng Struct 188:493–505. https://doi.org/10.1016/j.engstruct.2019.03.029

Gentile R, Pampanin S, Raffaele D, Uva G (2019c) Non-linear analysis of RC masonry-infilled frames using the SLaMA method: part 1—mechanical interpretation of the infill/frame interaction and formulation of the procedure. Bull Earthq Eng 17(6):3283–3304. https://doi.org/10.1007/s10518-019-00580-w

Gentile R, Pampanin S, Raffaele D, Uva G (2019d) Non-linear analysis of RC masonry-infilled frames using the SLaMA method: part 2—parametric analysis and validation of the procedure. Bull Earthq Eng 17(6):3305–3326. https://doi.org/10.1007/s10518-019-00584-6

Hak S, Morandi P, Magenes G, Sullivan TJ (2012) Damage control for clay masonry infills in the design of RC frame structures. J Earthq Eng 16(1):1–35. https://doi.org/10.1080/13632469.2012.670575
Holmes M (1961) Steel frames with brickwork and concrete infilling. ICE Proc 19(4):473–478
Kent DC, Park R (1971) Flexural members with confined concrete. J Struct Eng 97:1969–1990
Koutromanos I, Kyriakides M, Stavridis A et al (2013) Shake-table tests of a 3-story masonry-infilled RC frame retrofitted with composite materials. J Struct Eng 139:1340–1351. https://doi.org/10.1061/(asce)st.1943-541x.0000689
Liauw TC, Kwan KH (1984) Nonlinear behaviour of non-integral infilled frames. Comput Struct 18:551–560
Magenes G, Pampanin S (2004) Seismic response of gravity-load design frames with masonry infills. In: Proceedings of the 13th world conference on earthquake engineering Vancouver
Mainstone RJ (1974) Supplementary note on the stiffness and strengths of infilled frames. Building Research Station, Garston
Marini A, Passoni C, Belleri A, Feroldi F, Preti M, Metelli G, Riva P, Giuriani E, Plizzari G (2017) Combining seismic retrofit with energy refurbishment for the sustainable renovation of RC buildings: a proof of concept. Eur J Environ Civ Eng 8189:1–21. https://doi.org/10.1080/19648189.2017.1363665
Marinković M, Butenweg C (2019) Innovative decoupling system for the seismic protection of masonry infill walls in reinforced concrete frames. Eng Struct. https://doi.org/10.1016/j.engstruct.2019.109435
Marinković M, Butenweg C (2022) Experimental testing of decoupled masonry infills with steel anchors for out-of-plane support under combined in-plane and out-of-plane seismic loading. Constr Build Mater. https://doi.org/10.1016/j.conbuildmat.2021.126041
Matthews J, Bull D, Mander J (2003) Hollowcore floor slab performance following a severe earthquake. In: Proceedings of the 2003 fib symposium, concrete structures in seismic regions
Mazza F (2019) In-plane–out-of-plane non-linear model of masonry infills in the seismic analysis of R.C.-framed buildings. Earthq Eng Struct Dyn 48:432–453. https://doi.org/10.1002/eqe.3143
Mehrabi AB, Shing PB, Schuller MP, Noland JL (1996) Experimental evaluation of masonry-infilled RC frames. J Struct Eng 122(3):228–237. https://doi.org/10.1061/(asce)0733-9445(1996)122:3(228)
Milanesi RR, Morandi P, Magenes G (2018a) Local effects on RC frames induced by AAC masonry infills through FEM simulation of in-plane tests. Bull Earthq Eng 16:4053–4080. https://doi.org/10.1007/s10518-018-0353-5
Milanesi RR, Morandi P, Penna A, Magenes G (2018b) Seismic performance of AAC masonry infill: From traditional systems to innovative solutions. In: Ce/Papers, pp 311–317
Morandi P, Hak S, Magenes G (2018a) Performance-based interpretation of in-plane cyclic tests on RC frames with strong masonry infills. Eng Struct 156:503–521. https://doi.org/10.1016/j.engstruct.2017.11.058
Morandi P, Milanesi RR, Magenes G (2018b) Innovative solution for seismic-resistant masonry infills with sliding joints: in-plane experimental performance. Eng Struct 176:719–733. https://doi.org/10.1016/j.engstruct.2018.09.018
Morandi P, Hak S, Milanesi RR, Magenes G (2022) In-plane/out-of-plane interaction of strong masonry infills: From cyclic tests to out-of-plane verifications. Earthq Eng Struct Dyn 51:648–672. https://doi.org/10.1002/eqe.3584
Moretti ML, Papatheocharis T, Perdikaris PC (2014) Design of reinforced concrete infilled frames. J Struct Eng 140:04014062. https://doi.org/10.1061/(asce)st.1943-541x.0001042
NZSEE (2006) Assessment and improvement of the seismic performance of existing buildings. New Zealand Society for Earthquake Engineering, Wellington
NZSEE (2017) The seismic assessment of existing buildings—technical guidelines for engineering assessments. New Zealand Society for Earthquake Engineering, Wellington
Pampanin S (2006) Controversial aspects in seismic assessment and retrofit of structures in modern times: Understanding and implementing lessons from ancient heritage. Bull New Zeal Soc Earthq Eng 39:120–134. https://doi.org/10.5459/bnzsee.39.2.120-133
Pampanin S (2017) Towards the practical implementation of performance-based assessment and retrofit strategies for RC buildings: challenges and solutions. In: Proceedings of the 4th conference on smart monitoring, assessment and rehabilitation of civil structures, Zurich, Switzerland
Pampanin S, Calvi GM, Moratti M (2002) Seismic behaviour of RC Beam-column joints designed for gravity loads. In: Proceedings of the12th European conference on earthquake engineering, London, UK.
Pampanin S, Magenes G, Carr A (2003) Modelling of shear hinge mechanism in poorly detailed RC beam–column joints. In: Proceedings of the 2003 fib symposium. fib, Athens
Pampanin S, Bolognini D, Pavese A (2007) Performance-based seismic retrofit strategy for existing reinforced concrete frame systems using fiber-reinforced polymer composites. J Compos Constr 11:211–226. https://doi.org/10.1061/(ASCE)1090-0268(2007)11:2(211)

Papia M, Cavaleri L, Fossetti M (2003) Infilled frames: developments in the evaluation of the stiffening effect of infills. Struct Eng Mech 16(6):675–693

Pashaie MR, Mohammadi M (2021) An extended multiple-strut model to estimate infill effects on multi-storey steel frames with different connection rigidities. Structures 30:710–734. https://doi.org/10.1016/j.istruc.2020.12.035

Paulay T, Pristley MJN (1992) Seismic design of reinforced concrete and masonry buildings. Wiley, New York

Pedone L, Bianchi S, Giovinazzi S, Pampanin S (2022) A framework and tool for knowledge-based seismic risk assessment of school buildings: SLaMA-School. Sustainability 14:9982. https://doi.org/10.3390/SU14169982

Peng BHH, Dhakal RP, Fenwick RC, Carr AJ, Bull DK (2011) Elongation of plastic hinges in ductile RC members: model development. J Adv Concr Technol 9(3):315–326. https://doi.org/10.3151/jact.9.315

Polyakov SV (1960) On the interaction between masonry filler walls and enclosing frame when loading in the plane of the wall. In: Translation in earthquake engineering, EERI, San Francisco, pp 36–42

Preti M, Migliorati L, Giuriani E (2015) Experimental testing of engineered masonry infill walls for post-earthquake structural damage control. Bull Earthq Eng 13:2029–2049. https://doi.org/10.1007/s10518-014-9701-2

Priestley MJN, Calvi GM, Kowalsky MJ (2007) Displacement-based seismic design of structures. IUSS Press, Pavia

RD 2229 (1939) Regio Decreto Legge n. 2229 del 16/11/1939. Gazzetta Ufficiale della Repubblica Italiana n.92, 18/04/1940. Consiglio dei Minitri, Rome, Italy (**in Italian**)

Ricci P, Di Domenico M, Verderame GM (2018) Experimental assessment of the in-plane/out-of-plane interaction in unreinforced masonry infill walls. Eng Struct 173:960–978. https://doi.org/10.1016/j.engstruct.2018.07.033

Sansoni C, da Silva LCM, Marques R, Pampanin S, Lourenço PB (2022) SLaMA-URM method for the seismic vulnerability assessment of UnReinforced Masonry structures: formulation and validation for a substructure. J Build Eng. https://doi.org/10.1016/j.jobe.2022.105487

Santarella L (1968) Prontuario del cemento armato. Hoepli, Milan (**in Italian**)

Stafford Smith B (1967) Methods for predicting the lateral stiffness and strength of multi-storey infilled frames. Build Sci 2(3):247–257

Sugano S (1996) State-of-the-art in techniques for rehabilitation of buildings. In: Proceedings of the11th world conference on earthquake engineering, Acapulco, Mexico, pp 1–16

Taghavi S, Miranda E (2003) Response assessment of nonstructural building elements. Pacific Earthquake Engineering Research Center, Berkley

Tang N, Dong L, Huang D, Xiao R (2019) Mechanical performance of polystyrene foam (EPS): experimental and numerical analysis. Polym Test 73:359–365. https://doi.org/10.1016/j.polymertesting.2018.12.001

Tasligedik AS, Pampanin S (2017) Rocking cantilever clay brick infill wall panels: a novel low damage infill wall system. J Earthq Eng 21(7):1023–1049. https://doi.org/10.1080/13632469.2016.1190797

Tasligedik AS, Akguzel U, Kam WY, Pampanin S (2018) Strength hierarchy at reinforced concrete beam–column joints and global capacity. J Earthq Eng 22:454–487. https://doi.org/10.1080/13632469.2016.1233916

Taylor L (2004) Vertical displacement incompatibility between floor slabs and seismic resisting systems. BE Thesis, University of Canterbury, Christchurch, New Zealand

Tsantilis AV, Triantafillou TC (2018) Innovative seismic isolation of masonry infills using cellular materials at the interface with the surrounding RC frames. Eng Struct. https://doi.org/10.1016/j.engstruct.2017.11.025

Vides R, Pampanin S (2015) Towards a performance-based design of precast concrete diaphragms using jointed dissipative connectors: concept and feasibility study. In: Proceedings of the 2015 NZSEE Conference. Rotorua, New Zealand: New Zealand Society for Earthquake Engineering (NZSEE).

Wararuksajja W, Srechai J, Leelataviwat S (2020) Seismic design of RC moment-resisting frames with concrete block infill walls considering local infill-frame interactions. Bull Earthq Eng 18:6445–6474. https://doi.org/10.1007/s10518-020-00942-9

Zamic R, Tomazevic M (1984) The behaviour of masonry infilled reinforced concrete frames subjected to cyclic lateral loading. In: Proceedings of the 8th world conference on earthquake engineering. Prentice-Hall, San Francisco

Zhu M, McKenna F, Scott MH (2018) OpenSeesPy: python library for the OpenSees finite element framework. SoftwareX 7:6–11. https://doi.org/10.1016/j.softx.2017.10.009